Generation and confinement of hot ions and electrons in a reversed-field pinch plasma

2010 Plasma Phys. Control. Fusion 52 124048

(http://iopscience.iop.org/0741-3335/52/12/124048)

Plasma Phys. Control. Fusion **52** (2010) 124048 (14pp) doi:10.1088/0741-3335/52/12/124048

Generation and confinement of hot ions and electrons in a reversed-field pinch plasma

B E Chapman[1], A F Almagri[1], J K Anderson[1], D L Brower[2], K J Caspary[1], D J Clayton[1], D Craig[3], D J Den Hartog[1], W X Ding[2], D A Ennis[1], G Fiksel[1,4], S Gangadhara[1], S Kumar[1], R M Magee[1], R O'Connell[1], E Parke[1], S C Prager[1], J A Reusch[1], J S Sarff[1], H D Stephens[1] and Y M Yang[1]

[1] Department of Physics, University of Wisconsin, Madison, WI 53706, USA
[2] Department of Physics and Astronomy, University of California, Los Angeles, CA 90095, USA
[3] Wheaton College, Wheaton, IL 60187, USA

E-mail: bchapman@wisc.edu

Received 19 June 2010, in final form 14 October 2010
Published 15 November 2010
Online at stacks.iop.org/PPCF/52/124048

Abstract

By manipulating magnetic reconnection in Madison Symmetric Torus (MST) discharges, we have generated and confined for the first time a reversed-field pinch (RFP) plasma with an ion temperature >1 keV and an electron temperature of 2 keV. This is achieved at a toroidal plasma current of about 0.5 MA, approaching MST's present maximum. The manipulation begins with intensification of discrete magnetic reconnection events, causing the ion temperature to increase to several kiloelectronvolts. The reconnection is then quickly suppressed with inductive current profile control, leading to capture of a portion of the added ion heat with improved ion energy confinement. Electron energy confinement is simultaneously improved, leading to a rapid ohmically driven increase in the electron temperature. A steep electron temperature gradient emerges in the outer region of the plasma, with a local thermal diffusivity of about $2\,m^2\,s^{-1}$. The global energy confinement time reaches 12 ms, the largest value yet achieved in the RFP and which is roughly comparable to the H-mode scaling prediction for a tokamak with the same plasma current, density, heating power, size and shape.

1. Introduction

The reversed-field pinch (RFP) is a toroidal magnetically confined fusion plasma distinguished in part by its toroidal magnetic field, which is reversed in the plasma edge relative to its

[4] Present address: Laboratory for Laser Energetics, University of Rochester, 250 East River Road, Rochester, NY 14623, USA.

direction in the plasma core. This plasma is also characterized by multiple resonant surfaces where magnetic tearing and reconnection can occur. In the plasma core are resonant surfaces for tearing modes with poloidal mode number $m = 1$. At a single radius closer to the plasma boundary is the resonance location for tearing modes with $m = 0$. This location is the toroidal field reversal radius, across which the toroidal field reverses. Collectively, these modes produce a number of strong effects on the plasma, two of which are important here: energy transport and collisionless ion heating.

The dominant $m = 1$ modes are driven unstable by a gradient in the radial profile of the plasma current. The tearing and reconnection associated with these modes leads to a stochastic magnetic topology in the core, which in turn produces rapid transport, with a central electron thermal diffusivity of several hundred $\mathrm{m}^2\,\mathrm{s}^{-1}$ [1, 2]. The $m = 1$ mode amplitudes and degree of stochasticity increase rapidly and substantially during magnetic reconnection events, or sawtooth crashes. During these events, the $m = 0$ modes are also driven to large amplitude by nonlinear coupling with the $m = 1$ modes [3, 4]. In the Madison Symmetric Torus (MST) [5] RFP, these reconnection events occur periodically throughout most discharges, each event lasting only about 100 μs. Given the increase in stochasticity in the plasma core, each of these events causes a rapid drop in the central electron temperature [6]. However, the ion temperature usually increases, sometimes by several hundred percent [7–9]. Substantial ion heating has been linked to reconnection in other RFP devices as well [10–14], and both particle acceleration and heating are commonly associated with reconnection in magnetized astrophysical and space plasmas such as the solar corona [15] and the earth's magnetosphere [16]. In MST, the ion temperature increase occurs globally due to the large number of reconnection sites in the plasma, but heating due to the $m = 1$ modes in the core occurs only when the $m = 0$ modes are involved in the reconnection event [8, 9]. Reconnection events occur occasionally in which there is activity in only the $m = 1$ modes. In such cases, no additional ion heating is observed anywhere in the plasma. When heating does occur, it always corresponds to a drop in the stored magnetic energy. Reconnection facilitates the conversion of magnetic energy to ion thermal energy, and recent measurements on MST in plasmas produced from different working gases (hydrogen, deuterium and helium, separately) reveal that the fraction of magnetic energy appearing as ion thermal energy increases as the square root of the ion mass [17].

In this paper, we demonstrate manipulation of magnetic reconnection in the MST for two purposes. The first is intensification of ion heating during reconnection events. The second is the subsequent sustained reduction of both ion and electron energy loss. The ion heating during reconnection events is intensified primarily with a relatively small adjustment to the magnetic equilibrium. This causes the rapid generation of a multi-kiloelectronvolt ion temperature. Inductive modification of the current profile, a standard technique, immediately after such events then suppresses reconnection and stochasticity and reduces ion and electron energy transport. This allows the capture of a substantial fraction of the reconnection-based ion heat with a sustained central ion temperature >1 keV. It also allows a rapid ohmically driven increase in the electron temperature, reaching a maximum central value of about 2 keV. The generation of ion heat and subsequent initial suppression of reconnection occurs over a few milliseconds, during which time the amplitude of the tearing modes can vary by as much as 100-fold.

In plasmas with the highest electron temperature, steep gradients develop around the toroidal field reversal radius, corresponding to an electron thermal diffusivity of about $2\,\mathrm{m}^2\,\mathrm{s}^{-1}$. The largest gradient in the ion temperature profile also occurs in this region. Between the gradients in the electron temperature profile, centered on the reversal radius, is a flat region. The width of this region coincides roughly with the estimated width of an $m = 0$ island. The

$m = 0$ modes are calculated to be linearly unstable during the improved-confinement period, but their amplitudes are small.

Globally, the combined electron and ion energy confinement time is improved 12-fold (to 12 ms) relative to plasmas without reconnection suppression. This confinement time as well as the peak ion and electron temperatures are the largest values yet achieved in a RFP plasma with reconnection suppression. The energy confinement of these plasmas can also be described as approximately 'tokamak-like,' comparing with the H-mode scaling prediction for a tokamak with MST's plasma current, density, heating power, size and shape.

The balance of this paper is organized as follows. In section 2 we describe MST, the current profile control technique and two key diagnostics. The generation and capture of hot ions and electrons is demonstrated in sections 3 and 4. Sections 5 and 6 are devoted to local and global confinement improvement in these plasmas, including a comparison with confinement in tokamaks.

2. Experimental apparatus and diagnostics

The MST plasma has a major radius of 1.5 m and a minor radius of 0.5 m. The discharges described herein have a toroidal plasma current of about 0.5 MA, approaching the upper limit of MST's present current capability. The discharges are fueled with deuterium, with a central line-averaged electron density of about 10^{19} m^{-3}. The sole external means of plasma heating is ohmic dissipation due to the driven plasma current.

A key diagnostic for measurement of the ion temperature, T_i, in this work is based on charge-exchange-recombination spectroscopy (CHERS). As applied here, this diagnostic provides the temperature of fully stripped carbon ions at multiple radial locations (one location per discharge) with roughly 2 cm spatial resolution and a temporal resolution of 100 μs [18]. Another key diagnostic is multipoint, multipulse Thomson scattering [19]. A recent upgrade to this diagnostic now allows each of the diagnostic's two lasers to fire multiple times with a high repetition rate. As applied in this case, the electron temperature, T_e, profile is measured every 0.5 ms over a significant fraction of the discharge duration [20]. This capability is an important advance for high-β plasmas such as the RFP, for which a diagnostic based on the tokamak-standard electron-cyclotron-emission is not applicable.

Suppression of both the $m = 1$ and $m = 0$ tearing modes is achieved with a well-established technique for inductive control of the current profile [21, 22]. The key control parameter in this technique is the surface parallel electric field, $E_\parallel(a) = \boldsymbol{E} \cdot \boldsymbol{B}/B = (E_\theta B_\theta + E_\phi B_\phi)/B$, where E_θ and E_ϕ are the surface poloidal and toroidal electric fields, B_θ and B_ϕ are the surface poloidal and toroidal magnetic fields and B is the total surface magnetic field. Waveforms from a discharge utilizing this technique are shown in figure 1. The current profile control begins at about 10 ms, reflected by $E_\parallel(a)$ becoming positive in figure 1(a). From 10–18 ms, this current drive is effected through the toroidal magnetic field circuit. Four sets of capacitors are discharged in a preprogrammed sequence that causes B_ϕ to grow more and more negative. This reflects an increase in the stored magnetic energy, one consequence of the current profile control. This induces an E_θ which contributes positively to $E_\parallel$. The increase in B_ϕ affects strongly two RFP equilibrium parameters, the toroidal field reversal parameter, $F \equiv B_\phi(a)/\langle B_\phi \rangle$, and the pinch parameter, $\Theta \equiv B_\theta(a)/\langle B_\phi \rangle$, where $\langle B_\phi \rangle$ is the toroidal field averaged over the plasma cross section. These parameters, shown in figure 1, reach values much larger than in a typical MST plasma. The increase in the pinch parameter reflects a change in the plasma internal inductance, which is due in part to on-axis peaking of the current profile during this period. This central peaking was measured directly in MST several years ago with the application of current profile control roughly similar to that

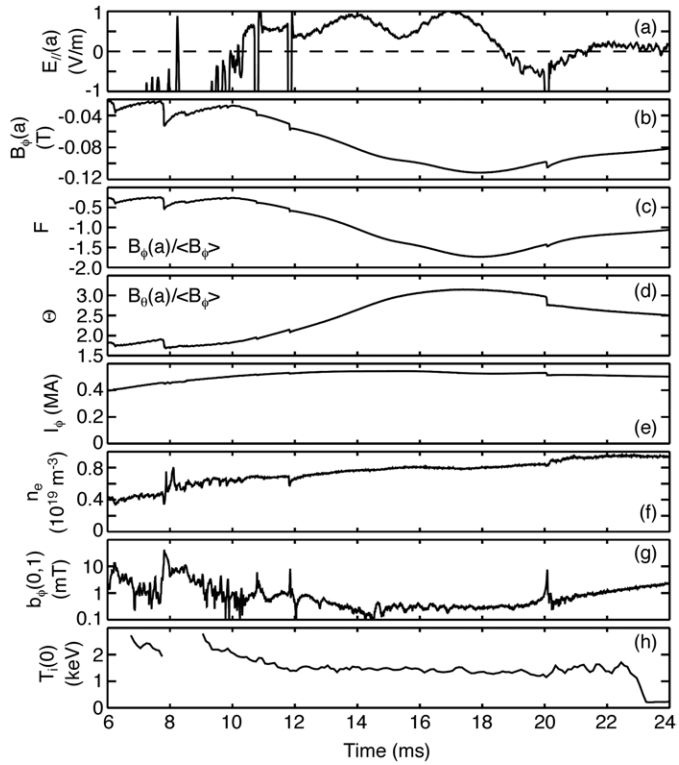

Figure 1. In a 0.5 MA discharge with inductive current profile modification beginning at 10 ms, time evolution of the (*a*) surface parallel electric field, (*b*) surface toroidal magnetic field, (*c*) reversal parameter, (*d*) pinch parameter, with suppressed zero on the vertical axis, (*e*) toroidal plasma current, (*f*) central line-averaged density, (*g*) amplitude of the $m = 0, n = 1$ tearing mode, plotted on a logarithmic scale and (*h*) central ion temperature. Mode amplitude measured with toroidal field sensing coils at plasma boundary. Apparent drop in ion temperature around 23 ms is an artifact of the diagnostic neutral beam termination. Shot number 1070829100.

described here [23]. This technique has been applied successfully in several RFP devices, but optimization continues [21, 22, 24–26].

Additional details concerning this technique as applied on MST can be found in a previous publication [27], but there is one notable difference between the waveform of $E_\parallel$ shown in figure 1 and that shown previously. The waveform previously consisted of triangular-shaped pulses, each corresponding to the discharge of one capacitor bank. The pulses in the present waveform are more rounded and, for the most part, longer lasting. This is due to the addition of an inductor in series with each capacitor bank. But for purposes of capturing reconnection-based ion heat, described in the next section, the inductor in series with the first capacitor bank is removed. This allows a faster rise in $E_\parallel$ and more effective capture of the added ion heat. This fast rise is discernible just after 10 ms in figure 1(*a*).

3. Achieving $T_i > 1$ keV

An example of intensified ion heating followed by capture of a portion of the ion heat is shown in figure 1, which contains the amplitude of the tearing mode with $m = 0$ and toroidal mode

number $n = 1$, as well the central ion temperature measured with CHERS. Occurring at around 6 and 8 ms in figure 1 are two global reconnection events corresponding to a rapid increase in both the $m = 0$ and $m = 1$ modes. During the event near 8 ms, the stored magnetic energy (not shown) drops by an estimated 34 kJ ($\sim$13%) in about 60 μs, implying a power greater than 500 MW. The magnetic energy is estimated with a simple equilibrium model based on measurements of the magnetic field at the plasma boundary [28]. A fraction of this power is channeled to the impurity and majority ions [17]. During the two events shown early in figure 1, the central T_i exceeds the upper range of the CHERS diagnostic, hence the gaps in the T_i data. However, T_i can be measured in the decay phase following each event, and these data imply that the central T_i may exceed 3 keV during heating. This is the largest ion temperature yet observed in the RFP, and it is achieved by operating simultaneously at large toroidal current and low density, and by increasing the degree of toroidal magnetic field reversal.

It has previously been demonstrated that, all else being equal, an increase in the toroidal current from 0.25 to 0.5 MA causes the central (carbon) ion temperature during reconnection events to roughly triple, reaching 1.5 keV [9]. Hence, the discharge shown in figure 1 has a toroidal plasma current of about 0.5 MA, figure 1(*e*). However, the degree of toroidal field reversal is also important. As the reversal parameter F approaches zero, corresponding to weak field reversal, the degree of ion heating during reconnection events is strongly diminished, even with large current. With $F = 0$, which also corresponds to an edge safety factor, $q(a) = 0$, the resonant surface for the $m = 0$ modes is removed from the plasma, and the heating is essentially eliminated. In contrast, stronger reversal can lead to much stronger ion heating. In the discharge shown in figure 1, F is about -0.25 between the large reconnection events. This corresponds to $q(a) = -0.05$. Hence, the degree of ion heating is sensitively dependent on the equilibrium. A similar relation between the reversal parameter and ion heating was also observed in the ZT-40M RFP [12]. Adjusting F to be more negative moves the $m = 0$ resonant surface further inside the plasma, and further away from the stabilizing influence of MST's thick conducting shell. This may facilitate more intense heating.

Low electron density is also important in the generation and capture of reconnection-based ion heat. The line-averaged density early in time in figure 1 is about 0.45×10^{19} m^{-3}, corresponding to about 8% of the Greenwald density limit [29]. With substantial toroidal field reversal, low density leads to periods where magnetic fluctuations are spontaneously reduced, and global energy confinement is somewhat improved [30]. Two such periods, which are characterized in part by periodic small bursts of $m = 0$ mode activity, occur after the large events in figure 1. These periods often terminate with reconnection events having particularly large mode amplitudes. Relative to typical MST plasmas, the ion temperature in plasmas such as that in figure 1 decays more slowly following reconnection heating. This may result in part from somewhat improved ion energy confinement following the reconnection events.

The combination of intensified heating and slower ion temperature decay allows capture of substantial ion energy with current profile control. In the discharge in figure 1, inductive modification of the current profile begins at 10 ms, leading to the eventual suppression of the $m = 1$ and $m = 0$ tearing modes, including the small bursts of $m = 0$ activity. The minimum amplitude of the $m = 0$, $n = 1$ mode during reconnection suppression is about 100 times smaller than its peak at 8 ms. The ion temperature in this plasma is sustained at greater than 1 keV with a small temperature decay rate. This is due in part to increased ion energy confinement. The global ion energy confinement time is roughly estimated to increase from 1 to 10 ms during reconnection suppression. This is based on a power balance calculation, including electron–ion heating and losses due to both convection and charge exchange. Charge exchange is one of the dominant channels of ion energy loss, and it is measured to drop roughly ten-fold. This is due to a drop in the neutral density which is precipitated by a drop in recycling of neutral

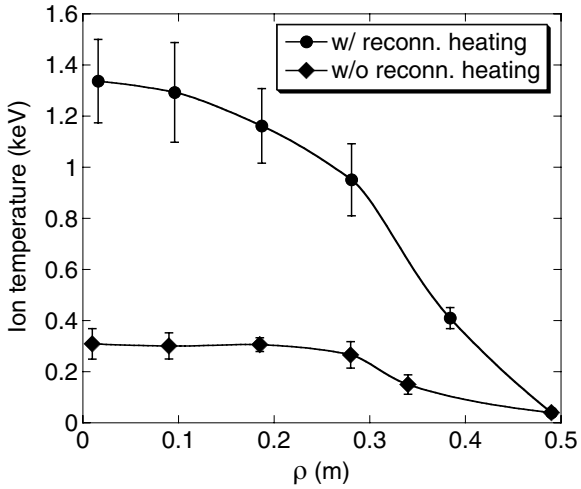

Figure 2. Shot-averaged ion temperature profiles near the end of improved-confinement periods with and without strong reconnection-based ion heating preceding the improved confinement. Magnitude of outermost data point in each profile is assumed. Error bars reflect standard deviation of shot average for each spatial point.

deuterium. Concurrent with this drop, the line-averaged electron density rises modestly, as shown in figure 1, reflecting an increase in density in the plasma core, and reflecting an overall improvement in particle confinement.

The capture of reconnection-based ion heat results in an ion temperature profile that is everywhere increased with respect to previous improved-confinement plasmas that did not exploit this form of ion heating. This is illustrated in figure 2. Given that the CHERS diagnostic provides the ion temperature at only one spatial point per discharge, the profiles shown in this figure are from an ensemble of similar discharges, approximately ten per spatial point. Both profiles were gathered late in periods of reconnection suppression, after several majority-impurity-ion equilibration times, in plasmas with the same toroidal plasma current (0.5 MA) and a line-averaged electron density ranging from 0.7×10^{19} to $1.0 \times 10^{19}\,\mathrm{m}^{-3}$, or 11% to 16% of the Greenwald density limit. The temperature profile resulting from reconnection heating was compiled at 20 ms in discharges like that in figure 1. With a Rutherford scattering diagnostic [31], the deuteron temperature was also measured at one location in these plasmas, confirming a large increase in the majority T_i.

Before closing this section, we note a degree of 'stiffness' in the ion temperature profile in MST. This is based on a comparison of T_i profiles from two plasma regimes, standard confinement and improved confinement, with central temperatures differing by almost a factor of four. The standard-confinement profile is extracted from figure 4 of a recently published paper on ion heating during reconnection in standard-confinement MST plasmas [8]. The improved-confinement profile is that with the larger temperature in figure 2 of this paper. Profile stiffness has long been noted in tokamak plasmas in both the ion and electron temperature profiles. See, for example, Mikkelsen *et al* [32] and Ryter *et al* [33], and references therein. Profile stiffness is linked to a critical gradient threshold, $\nabla T/T$, above which energy transport increases substantially. Over the spatial region where a profile is stiff, the profile shape does not vary as, e.g., the temperature at the periphery of the region varies. The central temperature is proportional to the temperature at the periphery. The apparent stiffness in MST T_i profiles is

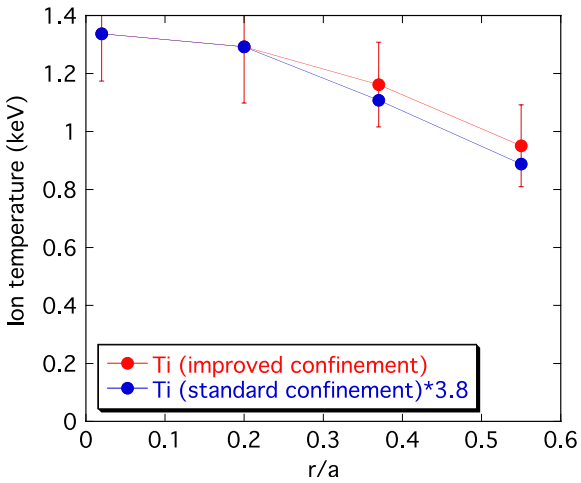

Figure 3. Shot-averaged ion temperature profiles from improved-confinement and standard-confinement plasmas. Improved-confinement profile is from figure 2. Standard-confinement profile is average of data from −0.9 to −0.5 ms, inclusive, in figure 4 of [8]. Standard profile scaled such that innermost data point is identical to that of the improved-confinement profile. Data plotted versus impact parameter of CHERS diagnostic chords. Error bars reflect standard deviation of shot average for each spatial point. Error bars for standard-confinement profile about the size of the plot symbols.

shown in figure 3. The standard-confinement profile was compiled several milliseconds after ion-heating reconnection events, somewhat akin to the improved-confinement profile. The significance, or lack thereof, of this profile stiffness remains to be determined, particularly given the dominance of current-gradient-driven stochastic magnetic transport in standard plasmas. A similar comparison of the two improved-confinement T_i profiles in figure 2 also shows a degree of stiffness, but there is greater disparity in the profile shapes.

4. Achieving $T_e \sim 2$ keV

With the recent advance in Thomson scattering on MST, we can now compare the temporal evolution of T_i and T_e in a single discharge. In figure 4 are the central ion and electron temperatures from a discharge similar to that in figure 1. As in figure 1, current profile control is applied at 10 ms, preceded by intense ion heating. Fluctuations are reduced, and confinement improved, just before 13 ms. The ion temperature slowly decays during this period, while the electron temperature ramps up strongly. This ramp continues until the end of the reduced fluctuation period at around 20 ms. This is encouraging for the application of inductive current profile control in RFP plasmas with even larger toroidal current. Since the profile control depends on the rampdown of toroidal flux, the duration of the control is limited by the amount of toroidal flux initially embedded in the plasma. For a given equilibrium, the embedded flux increases with toroidal current. Hence, larger toroidal current implies longer current profile control. Larger current will be possible in MST with a proposed upgrade to MST's poloidal field power supply. The data in figure 4 also illustrate clearly the fact that the ions and electrons are largely thermally independent in these plasmas. The large electron temperature and low plasma density lead to an electron–ion energy equilibration time of hundreds of milliseconds, much longer than the present duration of improved confinement.

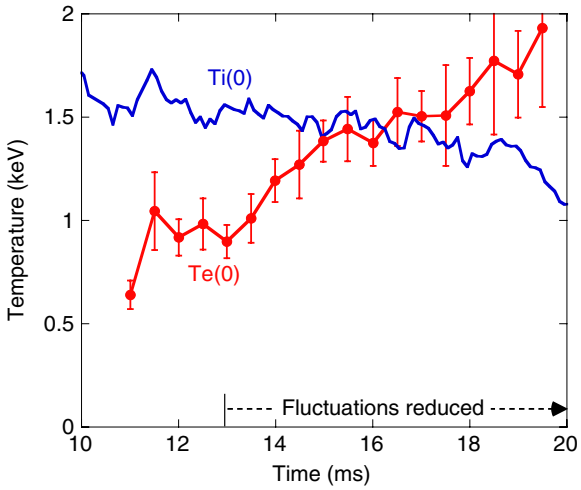

Figure 4. Temporal evolution of the central electron and ion temperatures in a discharge with current profile control beginning at 10 ms, and a period of reduced fluctuations beginning just before 13 ms, as indicated in the figure. Electron temperature measured every 0.5 ms. Error bars on electron temperature data derived from photon statistics for each time point. Shot number 1090415017.

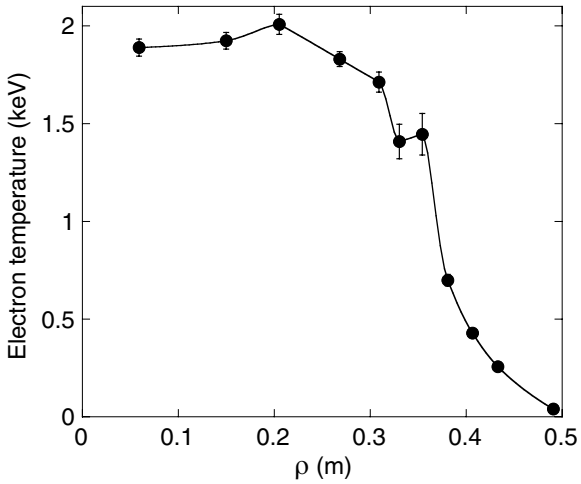

Figure 5. Electron temperature profile measured at 19.5 ms in the discharge shown in figure 1. Magnitude of outermost data point is estimated based on probe data from plasmas at lower plasma current.

The complete electron temperature profile was measured at 19.5 ms in the discharge in figure 1. This profile is shown in figure 5. The central temperature of about 2 keV represents a roughly four-fold increase over that (0.5 keV) achieved in MST plasmas at the same plasma current and electron density but without suppression of the tearing modes. In addition to the large central temperature, the shape of the T_e profile is also noteworthy. The profile is fairly flat in the core with a steep gradient in the region $\rho > 0.3$ m. The steep gradient is bisected by a narrow flattening roughly centered on the toroidal field reversal radius. This gradient, as

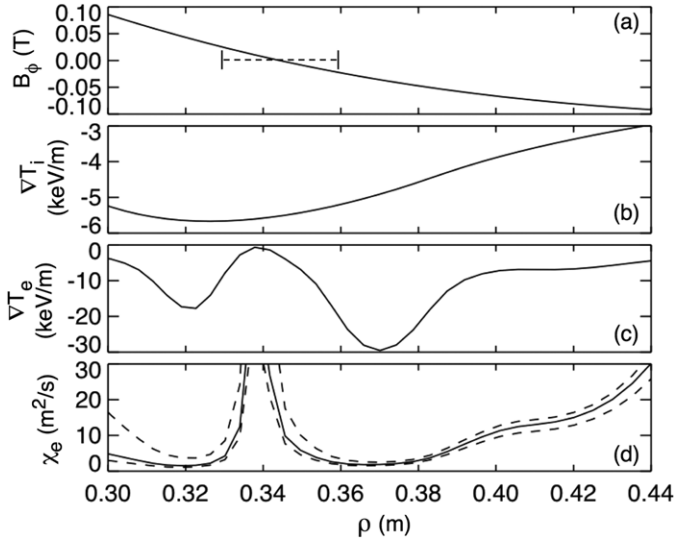

Figure 6. Radial profiles of (*a*) toroidal magnetic field, (*b*) ion temperature gradient associated with reconnection-heated profile in figure 2 and (*c*)–(*d*) electron temperature gradient and electron thermal conductivity associated with profile in figure 5. Estimated $m = 0$ island width indicated by dashed line in (*a*). Dashed lines in (*d*) represent estimated error. For (*c*) and (*d*), electron temperature profile is adjusted slightly around $\rho = 0.34$ such that the gradient remains negative everywhere.

well as a more modest gradient in the ion temperature profile, is discussed in more detail in the next section.

5. Local confinement improvement

Electron thermal diffusion is small in the large-gradient region of figure 5. This is illustrated in figure 6, which contains four profiles over a relatively narrow spatial extent. Profiles of the toroidal magnetic field, electron temperature gradient and electron thermal diffusivity, χ_e, are from the same shot and time as for the T_e profile in figure 5. The ion temperature gradient is from the high-temperature profile in figure 2, based on a shot average. The diffusivity associated with the two steep T_e gradients is about $2\,m^2\,s^{-1}$, likely the minimum value in the plasma. In the region $\rho > 0.4$ m, the diffusivity increases monotonically out to the plasma boundary and is substantially larger than $2\,m^2\,s^{-1}$. The diffusivity in the region $\rho < 0.3$ m is uncertain at present due in part to the apparent hollowness in the T_e profile. This may be an artifact of the small population of runaway electrons in the plasma core, but additional data are required to address this issue. The region with two steep gradients coincides with the toroidal field reversal radius, where $B_\phi = 0$ and $q = 0$. In addition to the large gradients in T_e, we note that the coarsely measured T_i profile also exhibits its largest gradient in the vicinity of $q = 0$.

It is quite possible that the two regions of minimum χ_e are magnetically stochastic. The $m = 1$ modes resonant in this region have $|n| > 35$, and their respective resonant surfaces are spaced less than 0.001 m apart. Hence, even if these modes are of small amplitude, overlap of their respective magnetic islands is likely. Even so, stochastic electron energy transport scales as the square of the mode amplitude [34], so if the mode amplitudes are sufficiently small, stochastic transport may be small as well.

The local flattening in the T_e profile shown in figure 5 implies locally large transport. This region coincides with the $q = 0$ surface, and the width of this region is roughly consistent with that of an $m = 0$ island structure. The estimated island width, W, is shown in figure 6(a) and is calculated from $W = 4\sqrt{(r_s b_r)/(nB_\theta q')}$, where r_s is the radius of the mode resonant surface, b_r is the radial magnetic perturbation at r_s, n is the toroidal mode number, B_θ is the equilibrium field at r_s and q' is the radial derivative of q at r_s [35]. The quantities r_s, B_θ and q' are calculated based on reconstruction of the magnetic equilibrium using MSTFit [36]. These reconstructions are constrained not only by internal and external magnetic measurements, but also by measurements of quantities such as temperature and density. The radial field perturbation at r_s is estimated using the output of the linear stability code, RESTER [37], which allows one to calculate b_r at the resonant surface based on the measured toroidal field perturbation at sensing coils located at the MST plasma boundary. There are multiple resonant $m = 0$ modes of finite amplitude in this plasma. For this estimate, we consider the single largest mode, which in this case has $n = 3$, and arrive at $W \cong 3$ cm. Note that while the $m = 0$ modes are calculated to be linearly unstable, their amplitudes are small during this period of improved confinement.

6. Global confinement improvement

The combination of large ion and electron temperatures, along with the simultaneously *reduced* ohmic input power of about 2.3 MW, results in a global energy confinement time $\equiv W_{th}/(P_{oh} - \mathrm{d}W_{th}/\mathrm{d}t)$ of about 12 ms. Here, W_{th} is the volume-integrated stored thermal energy and P_{oh} is the volume-integrated ohmic input power. In discharges without reconnection suppression but at the same plasma current and density as that described for the discharges here, P_{oh} is about 5 MW, and the energy confinement time is about 1 ms.

The improved energy confinement time quoted here is calculated near the end of the period of improved confinement, corresponding to the time of maximum electron temperature. In calculating the stored thermal energy, we used the electron and ion temperature profiles shown in figures 5 and 2, respectively. The electron density profile was measured in the same shot and at the same time as the electron temperature profile. The ion density profile is assumed to have the same shape as the electron density profile, but with a smaller magnitude to account for the estimated impurity dilution of the deuteron density. The ohmic input power is calculated in two ways. The first utilizes global power balance, subtracting from the total input power the time rate of change of the stored magnetic energy. The magnetic energy is derived from MSTFit. The second means of calculating the ohmic input power is based on simple Ohm's law, $P_{oh} = \int \eta J^2 \,\mathrm{d}V$, where η is the plasma resistance and J is the current density, calculated by MSTFit. The plasma resistance depends on T_e and Z_{eff}, the effective ionic charge. The latter quantity is determined from measurements of x-ray bremsstrahlung [38]. Both approaches to calculation of the ohmic input power provide the same result.

The improved-confinement time of 12 ms is achieved at a total beta, $\beta_{tot} = \langle p \rangle / [B^2(a)/2\mu_o]$, of about 10%, where $\langle p \rangle$ is the volume-averaged plasma pressure and $B(a)$ is the total (poloidal + toroidal) field at the plasma boundary. This is well below the present maximum beta of 26% achieved in MST at lower current and much higher density [39, 40]. Beta in the present discharges is limited in part by the relatively small ohmic heating power.

The previous best confinement time in MST was about 10 ms, also achieved with inductive current profile control, but at substantially lower plasma current, 0.2 MA, and with lower maximum temperatures, $T_e(0) \sim 0.6$ keV and $T_i(0) \sim 0.2$ keV [22]. This confinement time was compared with what is predicted by the IPB98(y,2) ELMy H-mode tokamak confinement scaling, using relevant MST discharge parameters in the scaling formula [41, 42]. The formula

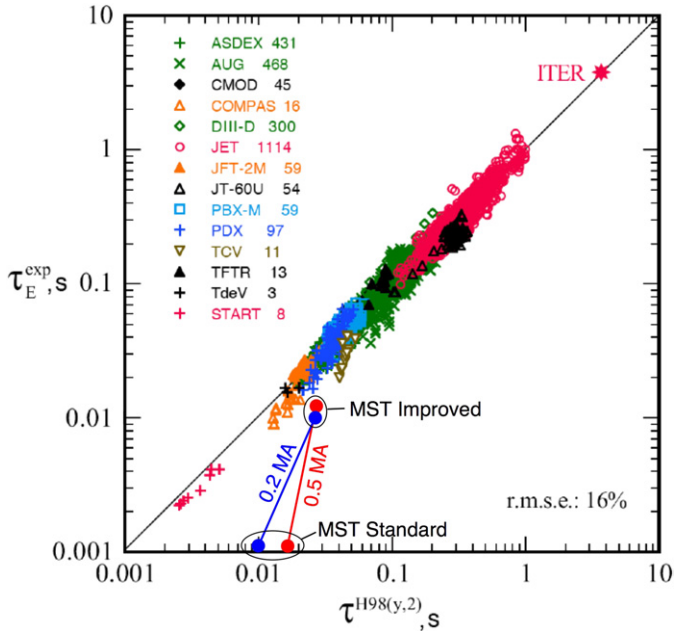

Figure 7. MST confinement compared with a 'fiducial' tokamak specified by the IPB98(y,2) ELMy-H mode empirical scaling (reprinted from ITER Physics Guidelines, ITER report N 19 FDR 1 01-07-13 R 0.1).

is $\tau = (0.0562) I_\phi^{0.93} B_\phi^{0.15} P^{-0.69} n^{0.41} M^{0.19} R^{1.97} \varepsilon^{0.58} \kappa^{0.78}$, where P is the loss power, n is the line-averaged density, M is the average ion mass, R is the major radius, ε is the inverse aspect ratio and κ is the elongation. The tokamak data underlying this scaling come from the ITER physics database [43]. To compute data points for MST, most MST parameters were input directly into the formula. However, for B_ϕ, an equivalent tokamak field was used given MST's plasma current and the assumption that $q(a) = 4$. This same methodology is applied for the present-day 0.5 MA MST plasmas, requiring an equivalent tokamak field at the plasma boundary of about 2.5 T. Fortunately, the scaling dependence on the toroidal field is weak.

MST standard- and improved-confinement data are overlaid with the tokamak database in figure 7. The two data points in blue are those reported previously for 0.2 MA plasmas [41, 42]. The two data points in red are new additions for the 0.5 MA plasmas described in this paper. Both of the improved-confinement data points lie within about a factor of two of the scaling prediction. Note that this simple comparison is not meant to imply that this or other tokamak confinement scalings apply to the RFP. Instead it is meant to demonstrate that the best RFP energy confinement is roughly comparable to that achieved in an equivalent tokamak, but with a much smaller toroidal field. As shown in figure 1(*b*), $B_\phi \sim 0.1$ T in these 0.5 MA MST plasmas.

7. Summary and discussion

We have demonstrated here the extension of improved confinement in MST to higher plasma current (near the upper bound of MST's present capability) and higher ion and electron temperatures. Among the potential reactor attributes of the RFP is ohmic heating to ignition. This is based on the RFP plasma's relatively large electrical resistance. The RFP still has

far to go toward reactor-relevant temperatures, but results thus far imply that even higher temperatures than those shown here should be possible at larger plasma current.

Not only do these plasmas represent an advance in fusion performance, but their characterization has benefited tremendously from improvements in MST's diagnostic set, particularly with respect to measurement of the electron temperature. The gradients that form in the electron, and ion, temperature profiles suggest the importance of the region around the toroidal field reversal radius. Particularly for the electrons, it appears that this region acts as an energy transport barrier. The shape of the T_e profile in figure 5 is roughly similar to that of T_e profiles measured previously in lower-current discharges with the aforementioned 10 ms confinement time [22]. The Thomson scattering system at that time provided the electron temperature at only one spatial and temporal point per shot. Hence, compilation of complete profiles, based on shot averaging, required many, many shots. Nonetheless, these older profiles were fairly flat in the core with a substantial T_e gradient just beyond $\rho = 0.3$ m. For a given plasma current, this profile shape has thus far been associated with the largest central electron temperatures and energy confinement times.

It has been demonstrated that to maximize T_e and energy confinement, one must control not only the centrally resonant $m = 1$ tearing modes, but also the $m = 0$ and nearby high-n $m = 1$ modes [22, 42]. A possible reason for this is provided by the data described above. If the $m = 0$ or nearby $m = 1$ modes are destabilized, one can easily imagine an interruption of the transport barrier, thereby adversely affecting the electron temperature and energy confinement further inside the plasma. This notion is supported by the temporal evolution of the soft-x-ray emission profile during small $m = 0$ bursts occurring during periods of spontaneously improved confinement in MST [44]. With each burst, x-ray emission is observed to decrease from the edge to the core, corresponding to an inward propagating 'cold pulse.'

It has previously been demonstrated in plasmas such as those described here that magnetic stochasticity has been substantially reduced in the plasma core. One piece of evidence for this was obtained via the diagnosis of high-energy (100 keV) runaway electrons [45]. The rate of transport in a stochastic field increases with particle velocity, so the mere existence of such high-energy particles is suggestive. But their rate of transport was measured directly and found to be velocity independent. Another piece of evidence was acquired with x-ray tomography, which revealed the presence of two distinct, non-overlapping islands in the core of these plasmas [46]. Given that energy transport is still finite in these plasmas, some other transport mechanism, possibly rooted in electrostatic fluctuations, must be playing a role. Such a mechanism may play a role in, e.g., the relatively flat central electron temperature profile.

Although it has now been demonstrated with current profile control that energy confinement can be improved substantially over essentially the entire range of plasma current accessible to MST, the degree of improvement so far increases only modestly with current, figure 7. One potential reason for this is that the formerly measured 10 ms confinement time was achieved in conjunction with intensive boronization, but the present 12 ms confinement at higher current did not utilize boronization. Boronization is now being revived on MST so that we will be able to test its effect on energy confinement. Also important is that we have yet to identify the optimal waveform for the surface parallel electric field, and, hence, we have yet to identify the maximum energy confinement time of which MST is capable. To this end, we have just commissioned a solid-state programmable power supply for much improved control of the B_ϕ waveform. Further optimization of confinement and understanding how the confinement scales with, e.g., current and density is a major goal of the MST program.

Looking more broadly at the state of improved confinement in the RFP, at least three routes to improved confinement have been identified: the active profile control technique described in this paper and two routes that do not depend, at least explicitly, on profile control but are

instead self-organized (spontaneous), subject to certain operational conditions. One of these self-organized routes was first observed in TPE-1RM20 [47] and MST [30, 48] and depends in part on stronger-than-normal toroidal magnetic field reversal. But unlike inductive current profile control, the reversal parameter and overall magnetic equilibrium can remain nearly constant with time. Magnetic fluctuations are reduced in these plasmas, although not to the same degree as with active profile control. The other self-organized route, discovered recently in RFX-mod, appears to depend in part on the achievement of a relatively hot, low-resistance plasma, and once again the magnetic equilibrium can be steady [49]. This route is characterized by a single very large amplitude tearing mode in the core, with a reduction in the other core-resonant modes. Of these three routes, current profile control in MST has thus far led to the highest values of temperature, beta and energy confinement time. And this technique has led to substantial gains in other devices as well, with a five-fold improvement in energy confinement in TPE-RX [50]. The self-organized route depending on stronger magnetic field reversal has led to as much as a tripling of the energy confinement time, and the route characterized by a single large tearing mode has thus far led to a five-fold confinement improvement.

Acknowledgments

This work was made possible by the support of the entire MST team and by the US Department of Energy and the National Science Foundation.

References

[1] Fiksel G, Prager S C, Shen W and Stoneking M 1994 *Phys. Rev. Lett.* **72** 1028
[2] Biewer T M *et al* 2003 *Phys. Rev. Lett.* **91** 045004
[3] Assadi S, Prager S C and Sidikman K L 1992 *Phys. Rev. Lett.* **69** 281
[4] Choi S, Craig D, Ebrahimi F and Prager S C 2006 *Phys. Rev. Lett.* **96** 145004
[5] Dexter R N, Kerst D W, Lovell T W, Prager S C and Sprott J C 1991 *Fusion Technol.* **19** 131
[6] Biewer T M 2002 *PhD Thesis*, University of Wisconsin–Madison, Madison
[7] Scime E, Hokin S, Mattor N and Watts C 1992 *Phys. Rev. Lett.* **68** 2165
[8] Gangadhara S, Craig D, Ennis D A, Den Hartog D J, Fiksel G and Prager S C 2007 *Phys. Rev. Lett.* **98** 075001
[9] Gangadhara S, Craig D, Ennis D A, Den Hartog D J, Fiksel G and Prager S C 2008 *Phys. Plasmas* **15** 056121
[10] Howell R B and Nagayama Y 1985 *Phys. Fluids* **28** 743
[11] Carolan P G, Field A R, Lazaros A, Rusbridge M G, Tsui H Y W and Bevir M K 1987 *Proc. 14th European Conf. on Controlled Fusion and Plasma Physics (Madrid, Spain)* (Petit-Lancy: European Physical Society) vol 2 p 469
[12] G A Wurden *et al* 1988 *Proc. 15th European Conf. on Controlled Fusion and Plasma Physics (Dubrovnik, Croatia)* (Petit-Lancy: European Physical Society) p 533
[13] Fujisawa A, Ji H, Yamagishi K, Shinohara S, Toyama H and Miyamoto K 1991 *Nucl. Fusion* **31** 1443
[14] Horling P, Hedinz G, Brzozowskiz J H, Tennforsz E and Mazur S 1996 *Plasma Phys. Control. Fusion* **38** 1725
[15] Priest E R, Foley C R, Heyvaerts J, Arber T D, Culhane J L and Acton L W 1998 *Nature* **393** 545
[16] Phan T D, Sonnerup B U Ö and Lin R P 2001 *J. Geophys. Res.* **106** 25489
[17] Fiksel G, Almagri A F, Chapman B E, Mirnov V V, Ren Y, Sarff J S and Terry P W 2009 *Phys. Rev. Lett.* **103** 145002
[18] Den Hartog D J *et al* 2006 *Rev. Sci. Instrum.* **77** 10F122
[19] Reusch J A, Borchardt M T, Den Hartog D J, Falkowski A F, Holly D J, O'Connell R and Stephens H D 2008 *Rev. Sci. Instrum.* **79** 10E733
[20] Den Hartog D J *et al* 2010 *Rev. Sci. Instrum.* **81** 10D513
[21] Sarff J S, Hokin S A, Ji H, Prager S C and Sovinec C R 1994 *Phys. Rev. Lett.* **72** 3670
[22] Chapman B E *et al* 2001 *Phys. Rev. Lett.* **87** 205001
[23] Brower D L *et al* 2002 *Phys. Rev. Lett.* **88** 185005
[24] Bartiromo R, Martin P, Martini S, Bolzonella T, Canton A, Innocente P, Marrelli L, Murari A and Pasqualotto R 1999 *Phys. Rev. Lett.* **82** 1462

[25] Yagi Y, Maejima Y, Sakakita H, Hirano Y, Koguchi H, Shimada T and Sekine S 2002 *Plasma Phys. Control. Fusion* **44** 335
[26] Cecconello M, Malmberg J-A, Spizzo G, Chapman B E, Gravestjin R M, Franz P, Piovesan P, Martin P and Drake J R 2004 *Plasma Phys. Control. Fusion* **46** 145
[27] Chapman B E *et al* 2002 *Phys. Plasmas* **9** 2061
[28] Antoni V, Merlin D, Ortolani S and Paccagnella R 1986 *Nucl. Fusion* **26** 1711
[29] Greenwald M *et al* 1988 *Nucl. Fusion* **28** 2199
[30] Chapman B E, Chiang C-S, Prager S C, Sarff J S and Stoneking M R 1998 *Phys. Rev. Lett.* **80** 2137
[31] Reardon J C, Fiksel G, Forest C B, Abdrashitov A F, Davydenko V I, Ivanov A A, Korepanov S A, Murachtin S V and Shulzhenko G I 2001 *Rev. Sci. Instrum.* **72** 598
[32] Mikkelsen D R *et al* 2003 *Nucl. Fusion* **43** 30
[33] Ryter F *et al* 2001 *Plasma Phys. Control. Fusion* **43** A323
[34] Rechester A and Rosenbluth M 1978 *Phys. Rev. Lett.* **40** 38
[35] Bateman G 1980 *MHD Instabilities* (Cambridge, MA: MIT Press)
[36] Anderon J K, Forest C B, Biewer T M, Sarff J S and Wright J C 2004 *Nucl. Fusion* **44** 162
[37] Sovinec C R 1995 *PhD Thesis* University of Wisconsin–Madison, Madison
[38] Clayton D J 2010 *PhD Thesis* University of Wisconsin–Madison, Madison
[39] Wyman M D *et al* 2008 *Phys. Plasmas* **15** 010701
[40] Wyman M D *et al* 2009 *Nucl. Fusion* **49** 015003
[41] Sarff J S *et al* 2003 *Nucl. Fusion* **43** 1684
[42] Sarff J S *et al* 2003 *Plasma Phys. Control. Fusion* **45** A457
[43] ITER Physics Expert Groups on Confinement and Transport and Confinement Modeling and Database 1999 *Nucl. Fusion* **39** 2175
[44] Piovesan P, Almagri A, Chapman B E, Craig D, Marrelli L, Martin P, Prager S C and Sarff J S 2008 *Nucl. Fusion* **48** 095003
[45] O'Connell R *et al* 2003 *Phys. Rev. Lett.* **91** 045002
[46] Franz P, Marrelli L, Piovesan P, Chapman B E, Martin P, Predebon I, Spizzo G, White R B and Xiao C 2004 *Phys. Rev. Lett.* **92** 125001
[47] Hirano Y, Maejima Y, Shimada T, Hirota I and Yagi Y 1996 *Nucl. Fusion* **36** 721
[48] Chapman B E, Almagri A F, Cekic M, Den Hartog D J, Prager S C and Sarff J S 1996 *Phys. Plasmas* **3** 709
[49] Lorenzini R, Terranova D, Alfier A, Innocente P, Martines E, Pasqualotto R and Zanca P 2008 *Phys. Rev. Lett.* **101** 025005
[50] Yagi Y *et al* 2003 *Phys. Plasmas* **10** 2925